ENVIRONMENTAL RESEARCH
LETTERS

PURPOSE-LED PUBLISHING™ Part of the ENVIRONMENTAL RESEARCH SERIES

LETTER • OPEN ACCESS

Summertime warm extremes over the Indochina Peninsula linked to the tropical Indian Ocean tripole mode

To cite this article: Ning Meng *et al* 2025 *Environ. Res. Lett.* **20** 064030

View the article online for updates and enhancements.

You may also like

- Projected ENSO teleconnection on the Southeast Asian climate under global warming
Dzung Nguyen–Le
- Leading source and constraint on the systematic spread of the changes in East Asian and western North Pacific summer monsoon
Shijie Zhou, Ping Huang, Gang Huang et al.
- The variability and predictability of summer southwest monsoon intensity measurement index across mainland indochina: from local synoptic to large scale perspectives
Kyaw Than Oo, Yinshuo Dong and Kazora Jonah

This content was downloaded from IP address 211.64.159.223 on 20/05/2025 at 10:13

ENVIRONMENTAL RESEARCH
LETTERS

LETTER

Summertime warm extremes over the Indochina Peninsula linked to the tropical Indian Ocean tripole mode

Ning Meng[1,7], **Yang Yang**[1,7], **Bin Zuo**[2], **Yazhou Zhang**[1,*], **Jianping Li**[1,3,*], **Zhaolu Hou**[1], **Ting Liu**[4,5] and **Haili Wang**[6]

[1] State Key Laboratory of Physical Oceanography (POL)/Frontiers Science Center for Deep Ocean Multispheres and Earth System (FDOMES)/Key Laboratory of Physical Oceanography/Academy of the Future Ocean/College of Oceanic and Atmospheric Science, Ocean University of China, Qingdao, People's Republic of China
[2] Dalian Naval Academy, Dalian, People's Republic of China
[3] Laoshan Laboratory, Qingdao, People's Republic of China
[4] State Key Laboratory of Satellite Ocean Environment Dynamics, Second Institute of Oceanography, Ministry of Natural Resources, Hangzhou, People's Republic of China
[5] Southern Marine Science and Engineering Guangdong Laboratory (Zhuhai), Zhuhai, People's Republic of China
[6] State Key Laboratory of Tropical Oceanography (South China Sea Institute of Oceanology Chinese Academy of Sciences), Guangzhou, People's Republic of China
[7] Ning Meng and Yang Yang contributed equally to this work.
[*] Authors to whom any correspondence should be addressed.

E-mail: zyz@ouc.edu.cn and ljp@ouc.edu.cn

Keywords: tropical Indian Ocean tripole, Indochina Peninsula, warm extremes

Supplementary material for this article is available online

OPEN ACCESS

RECEIVED
12 March 2025

REVISED
27 April 2025

ACCEPTED FOR PUBLICATION
8 May 2025

PUBLISHED
20 May 2025

Original content from this work may be used under the terms of the Creative Commons Attribution 4.0 licence.

Any further distribution of this work must maintain attribution to the author(s) and the title of the work, journal citation and DOI.

Abstract

A new air–sea coupled variability of the sea surface temperature anomalies over the tropical Indian Ocean was observed and named as the tropical Indian Ocean tripole (IOT) in terms of its unique tripole pattern in recent studies, which peaks in boreal summer. This study found that the interannual variations of the warm extremes over the Indochina Peninsula during boreal summer can be affected by the IOT. When the positive IOT events occur, two cross-equatorial airflows are induced over the eastern and western tropical Indian Ocean, reinforcing the anomalous warm-humid westerly wind over the northern Indian Ocean. The water vapor convergence is strengthened and the anomalous middle-lower level negative geopotential height is formed over the Indochina Peninsula, leading to the local enhanced ascending motion and surplus precipitation, strongly supported by both observations and numerical simulation. These circulation anomalies favor the reduction of the local surface temperatures through increasing the cloud cover and hindering the downward solar radiation, further declining the warm extremes days. Improving to understand the warm extreme variations over the Indochina Peninsula and its impact factors is of great significance for local industrial development, agricultural production and human health.

1. Introduction

The Indochina Peninsula, located at the north of Southeastern Asia, not only is a key area connecting between the Indian Ocean and Pacific Ocean, but also occupies a central place on the Belt and Road Initiative of China (Chen and Li 2021, Liu *et al* 2021, Tritto and Camba 2022). In recent decades, the extreme temperatures with higher frequency and intensity and associated droughts occur over the Indochina Peninsula (Räsänen *et al* 2016, Huang *et al* 2018, Dang *et al* 2019, Fan *et al* 2022), significantly influencing the local human health (Matthews *et al* 2017, Mora *et al* 2017) and agriculture development (Zampieri *et al* 2017, Tebaldi and Lobell 2018). Since the most countries in Indochina Peninsula are densely populated and highly agriculture-reliant, the local lives and economies are more easily under great impacts of these temperature extremes (Tang 2019, Zander *et al* 2019). Hence, understanding deeply the variations in the extreme temperature and the possible causes over the Indochina Peninsula is both

© 2025 The Author(s). Published by IOP Publishing Ltd

essential to make decisions on development routes for the local governments and on future investment distributions along the Belt and Road for China.

The upward trend of the extreme temperatures over the Indochina Peninsula had attributed to the weakness of the Asian-Australian summer monsoon or anthropogenic forcing (Luo and Lau 2018, Li 2020, Dong *et al* 2021, Zhang *et al* 2021a, Fan *et al* 2022), whereas El Niño-Southern Oscillation (ENSO) was the most critical impact factor at the interannual timescale (Thirumalai *et al* 2017, Cheong *et al* 2018, Lin *et al* 2018). The developing El Niño in summer could intensify the downward motion over the Indochina Peninsula through modulating the Walker circulation and regional monsoon circulation (Yu *et al* 2023), resulting in the temperature extremes and further reinforcing the local continuous droughts (Hrudya *et al* 2021). Compared to the tropical Pacific, the tropical Indian Ocean variabilities, i.e. the Indian Ocean basin-warming (IOB) and Indian Ocean dipole (IOD), could also excite the anomalous anticyclone over the western North Pacific in the following summer (Yang *et al* 2007, Xie *et al* 2009), thereby influencing the temperature or extreme warm events in the Indochina Peninsula (Cheong *et al* 2018, Fan *et al* 2023).

However, Endo and Tozuka (2016) defined the canonical IOD and IOD Modoki referring to its spatial characteristic, which were characterized by zonal dipole and tripole patterns, respectively. On this basis, Zhang *et al* (2020) found that the IOD Modoki resembles the third leading mode (EOF3) of sea surface temperature (SST) in the tropical Indian Ocean. Moreover, the variance explained by the EOF3 is well separated with EOF2 and EOF4 according to the North's test (North *et al* 1982). Consequently, Zhang *et al* (2020) defined this EOF3 as the Indian Ocean tripole (IOT) mode, which was featured by the warm SST anomalies in the central tropical Indian Ocean and cold SST anomalies in the southeastern and western parts. The IOT generally develops in boreal late spring, peaks in boreal summer and decays in boreal fall, exhibiting an interannual variability. Based on the coupled oceanic–atmospheric bridge theory (Li *et al* 2019), subsequent studies further highlight the relatively independent contributions of the IOT on the surface air temperature over the western Tibetan Plateau and western United States and extreme low temperature in central Siberia in boreal summer (Zhang *et al* 2022a, 2022b, Zhu *et al* 2024). Overall, previous studies have mostly concentrated on the temperature or extreme conditions over the Indochina Peninsula associated with ENSO, IOB and IOD, whereas the interannual variability of the temperature extremes over there linked to the IOT remains unclear.

Therefore, this study investigates the spatial–temporal relationship between the IOT and summertime warm temperature extremes over the Indochina Peninsula, and elucidates the underlying physical mechanisms through observational analysis and numerical simulation. We will examine large-scale atmospheric circulation responses, including pathways of IOT forcing and their impacts on warm temperature extremes. Further, the mechanisms of IOT effects on temperature extremes will be evaluated in terms of atmospheric dynamics and thermal processes. Collectively, this will provide a more comprehensive understanding of the IOT's role in modulating summertime temperature variability over the Indochina Peninsula.

2. Datasets and methodology

2.1. Observational datasets

Two monthly indicators for extreme high temperatures during 1982–2018 on a 1.25° × 1.875° grid were utilized in this study: warm days (TX90p, percentage of time when daily max temperature >90th percentile) and warm nights (TN90p, percentage of time when daily min temperature >90th percentile), which were available at the World Meteorological Organization (Dunn *et al* 2020). The calculation method for TX90p is defined as follows: Let TX_{ij} be the daily maximum temperature on day i in period j and let $TX_{in}90$ be the calendar day 90th percentile centered on a 5 d window for the base period 1961–1990. The percentage of time for the base period is determined where $TX_{ij} > TXin90$ (www.climdex.org/learn/indices/#index-TX90p). TN90p follows the same method but uses the daily minimum temperature instead of TX.

The monthly mean atmosphere datasets for the period 1982–2018 were obtained from the National Centers for Environmental Prediction reanalysis (NCEP2) on a 2.5° × 2.5° grid (Kanamitsu *et al* 2002) and the European Centre for Medium-Range Weather Forecasts (ECMWF) Reanalysis version 5 (ERA5) on a 0.25° × 0.25° grid (Hersbach *et al* 2020). The atmospheric variables include 2 m temperature, atmosphere thickness, total cloud cover, and downward solar radiation flux in single level, and 10 levels (from 1000 to 200 hPa) horizontal wind, vertical wind, and geopotential height (HGT). The two precipitation datasets for same period with a 2.5° × 2.5° grid were also used in this study derived from the Climate Prediction Center Merged Analysis of Precipitation (CMAP, Xie and Arkin 1997) and the Global Precipitation Climatology Project (GPCP, Huffman *et al* 2015). Monthly oceanic SST data (1.0° × 1.0° horizontal resolution) during 1982–2018 from the Optimum Interpolation SST (OISST) was

used to extract the IOT (Reynolds *et al* 2002), which could also be validated by the improved Extended Reconstructed SST version 5 (ERSST v5) on a $2^\circ \times 2^\circ$ horizontal resolution (Huang *et al* 2017).

Anomalies were calculated as departures from the monthly climatology except TX90p and TN90p, and the long-term trends were removed from each dataset. To emphasize the interannual variation of the time-series of the IOT and temperature extremes, the 9 year high-pass filter were applied in this study via Butterworth filter. To quantify the impact of the IOT on temperature extremes, linear regression analysis was employed. Specifically, the regression coefficients of TX90p and TN90p onto the standardized IOT index were calculated over the Indochina Peninsula. These coefficients represent the change in extreme temperature days (TX90p/TN90p) per one standard deviation change in the IOT index.

To test the significance of correlations between variables X and Y, a two-tailed Student's t test using the effective number of degrees of freedom (N_{eff}) is used in this study, which is approximated as follows (Bretherton *et al* 1999, Li *et al* 2013, Zhang *et al* 2018, 2021b):

$$\frac{1}{N_{\text{eff}}} \approx \frac{1}{N} + \frac{2}{N}\sum_{i=1}^{N}\frac{N-i}{N}\rho_{XX}(i)\,\rho_{YY}(i),$$

where N is the total number of samples in the time series. $\rho_{XX}(i)$ and $\rho_{YY}(i)$ present the autocorrelations of the two time-series X and Y at time lag i, respectively.

2.2. Indices

The IOT mode index (TMI) is same as the Zhang *et al* (2020), which is the difference between averaged SST anomalies in the tropical central (65°–85° E, 5°–20° S) and southeastern (10° S–0°, 90°–110° E) and western (5° S–20° N, 45°–60° E and 10°–20° N, 60°–70° E) sectors of the Indian Ocean (figures 1(a) and (d)). The East Pacific ENSO, (Central Pacific ENSO or ENSO Modoki), IOB, IOD, and subtropical IOD indices are used to examine the relative independent effects of the IOT, which is listed in table S1 for definition.

2.3. Rossby wave ray

The far-field atmospheric response to large-scale forcing in the atmosphere is dominated by external Rossby waves. Stationary Rossby wave ray tracing is used in this study to reflect the stationary planetary and Rossby wave energy propagation originating from local forcing. Here, the stationary Rossby wave ray tracing was taken from Li *et al* (2015) and Zhao *et al* (2019), which are derived from the barotropic nondivergent vorticity equation and the basic flow is both zonal and meridional non-uniform in both latitude and longitude. Rossby wave ray tracing theory in horizontally nonuniform basic flows was used to track the trajectory of stationary Rossby wave trains and delineate the pathway of the influence of heat sources in southern tropical Asia (Li and Li 2012, Li *et al* 2015, Zhao *et al* 2015, 2019). Previous studies have shown that the dispersion relationship between Rossby wave frequency and wavenumber in horizontally non-uniform flows can be formulated as follows (Karoly 1983, Li and Nathan 1997, Li and Li 2012, Li *et al* 2015, Zhao *et al* 2015, 2019):

$$\omega = \overline{u}_{\text{M}}k + \overline{v}_{\text{M}}k + \frac{\overline{q}_x l - \overline{q}_y k}{k^2 + l^2}, \tag{1}$$

where ω is the wave frequency; k and l are the zonal and meridional wavenumbers, respectively; $(\overline{u}_{\text{M}}, \overline{v}_{\text{M}}) = (\overline{u}, \overline{v})/\cos\varphi$ is the Mercator projection of zonal and meridional winds; φ is the latitude; $\overline{q} = \nabla^2_{\text{M}}\overline{\psi}/\cos^2\varphi + f$ represents the absolute vorticity of the background; and $\overline{q}_x$ and $\overline{q}_y$ are the zonal and meridional gradients of $\overline{q}$, respectively. The total wavenumber is represented by $K = \sqrt{k^2 + l^2}$, and zonal and meridional components of the group velocity are as follows:

$$u_{\text{g}} = \frac{\partial\omega}{\partial k} = \overline{u}_{\text{M}} + \frac{\left(k^2 - l^2\right)\overline{q}_y - 2kl\overline{q}_x}{K^4}, \tag{2}$$

$$v_{\text{g}} = \frac{\partial\omega}{\partial l} = \overline{v}_{\text{M}} + \frac{\left(k^2 - l^2\right)\overline{q}_x - 2kl\overline{q}_y}{K^4},. \tag{3}$$

When the background flow varies along the ray, wavenumbers determined by the kinematic wave theory (Whitham 1960) can be expressed as follows:

$$\frac{\mathrm{d}_{\text{g}}k}{\mathrm{d}t} = -\frac{\partial\omega}{\partial x} = -k\frac{\partial\overline{u}_{\text{M}}}{\partial x} - l\frac{\partial\overline{v}_{\text{M}}}{\partial x} - \frac{1}{K^2}\left(l\frac{\partial\overline{q}_x}{\partial x} - k\frac{\partial\overline{q}_y}{\partial x}\right), \tag{4}$$

$$\frac{\mathrm{d}_{\text{g}}l}{\mathrm{d}t} = -\frac{\partial\omega}{\partial y} = -k\frac{\partial\overline{u}_{\text{M}}}{\partial y} - l\frac{\partial\overline{v}_{\text{M}}}{\partial y} - \frac{1}{K^2}\left(l\frac{\partial\overline{q}_x}{\partial y} - k\frac{\partial\overline{q}_y}{\partial y}\right) \tag{5}$$

where $\frac{\mathrm{d}_{\text{g}}}{\mathrm{d}t} = \frac{\partial}{\partial t} + \overline{u}_{\text{g}}\frac{\partial}{\partial x} + \overline{v}_{\text{g}}\frac{\partial}{\partial y}$ represents the material derivative moving with the group velocity. In equations (4) and (5), both zonal and meridional wavenumbers vary along the wave ray, which is a departure from classical theory (Hoskins and Karoly 1981). Termed as the wave ray tracing equation set, equations (2)–(5) allow determination of the initial local meridional wavenumber l after providing the initial position and zonal wavenumber, k, as in equation (1). Subsequently, the wave ray tracing equation set facilitates the derivation of the corresponding wave ray trajectory. For large-scale Rossby waves, integration ceases when the local meridional wavelength falls below 1000 km (Wang *et al* 2022, 2023).

2.4. Numerical experiments

Suggested by the previous studies (Zhang *et al* 2022a, 2022b), the precipitation anomalies over the southern tropical Asia (80°–125° E, 15°–25° N) act like an atmosphere bridge linking between the IOT and climate change in western United States and central Siberia. Therefore, we conducted numerical experiments to verify the responses of the precipitation over the southern tropical Asia to the IOT on using the CAM5 model. The CAM5 model used a 1.9° (lat)× 2.5° (lon) horizontal grid resolution and 26 hybrid sigma-pressure levels, and detailed information could refer to www.cesm.ucar.edu/models/cesm1.0/cam/docs/descriptio-n/cam5_desc.pdf. Here, we designed two CAM5 experiments with different lower boundary conditions: one control run and one positive IOT forcing sensitivity experiment. The control run was driven by climatological SST over the global oceanic domain. The positive IOT forcing was sets to the climatological SST plus the SST anomalies in the tropical Indian Ocean (40°–110° E, 20° S–20° N) that were extracted from positive IOT events in 1991, 1994, 2003, 2008, and 2011. Outside the tropical Indian Ocean, SST was set to monthly climatology. These two experiments were integrated for 33 years, with the first 3 years discarded as spin-up and the last 30 years used for analysis, which is same as Zhang *et al* (2020). It is noted that the forcing boundaries in the sensitive experiments was not treated, while it slightly affected the simulation results due to the high consistency in the precipitation and winds climatology between the observation and model (not shown).

3. Results

3.1. Spatiotemporal relationship between the IOT and warm extremes over the Indochina Peninsula

According to the prior studies (Zhang *et al* 2020, 2022a, 2022b, Zhu *et al* 2024), the IOT exhibits the evident seasonal phase-locking with a peak in JJA. To present the spatial features of the IOT, figure 1(a) displays the spatial feature of the SST anomalies related to the IOT in JJA over the tropical Indian Ocean. A significant tripole pattern is clearly observed in the tropical Indian Ocean, with the warm SST anomalies over the tropical central (65°–85° E, 5°–20° S) and southeastern (10° S–0°, 90°–110° E) and western (5° S–20° N, 45°–60° E and 10°–20° N, 60°–70° E) sectors of the Indian Ocean. The similar results are also robust using ERSST dataset (figure 1(b)). These suggest the unique spatial features of the IOT that is distinct with the IOB and IOD.

To explore the relationship between the IOT and warm extremes over the Indochina Peninsula, figures 1(c) and (d) show the spatial distribution of the warm days (TX90p) and warm nights (TN90p) associated with the IOT. The significant negative relations of the IOT with TX90p and TN90p occur over the Indochina Peninsula (figures 1(c) and (d)). The regression coefficient of the TX90p (TN90p) on the IOT area-averaged over the Indochina Peninsula is −2.23 (−1.95) days (figures 1(c) and (d)), implying that the TX90p (TN90p) decrease 2.23 (1.95) days when the IOT changes by one standard deviation. The high correlation coefficient between the IOT and TX90p (TN90p) area-averaged over the Indochina Peninsula is −0.58 (−0.58) at >0.01 significance level (figures 1(e) and (f)), and the explained variances of warm extremes by the IOT exceed 33%. These results indicate that the IOT is intrinsically associated with extreme high temperatures over the Indochina Peninsula. After removal of other SST modes in tropical Indian and Pacific Oceans, the correlation is still significant (figure S1).

3.2. Underlying physical mechanisms in observation

Generally, the surface temperature changes are strongly associated with the local atmosphere circulation variations. The anomalous higher or lower HGT may lead to warmer or cooler local surface temperature (Sun *et al* 2016, Li *et al* 2021). As a result, figure 1 presents the spatial correlations of the IOT with the HGT and wind anomalies in JJA using the ERA5 and NCEP2 datasets. The significant negative HGT anomalies related to the IOT are clearly observed at the whole troposphere over the Indochina Peninsula, accompanied by a strong cyclonic circulation (figure 2). The remarkable tropospheric circulation configuration associated with the IOT over the Indochina Peninsula is also conducive to the local water vapor convergence and upward movement, further enhancing convection activity (figure S2). Such anomalous circulation conditions over the Indochina Peninsula tend to increase the total cloud cover, to stop the downward solar radiation reaching the ground and to reduce the upward latent heat flux, thus causing a decline in the temperature of the middle–lower levels of the troposphere (figure 3), which further leads to the reduction of the surface temperature (figure S3). The high correlation coefficients between the surface temperature and warm extremes (TX90p and TN90p) are both −0.88 (figure S4), indicating that the IOT affects the local extreme high temperatures in the Indochina Peninsula by influencing the local surface temperature.

The mechanism by which the IOT affects the Indochina Peninsula circulation anomalies was investigated further. The aforementioned results indicate that the circulation anomalies associated with the IOT provide the favorable water vapor transport and dynamic conditions for the occurrence of precipitation over the Indochina Peninsula.

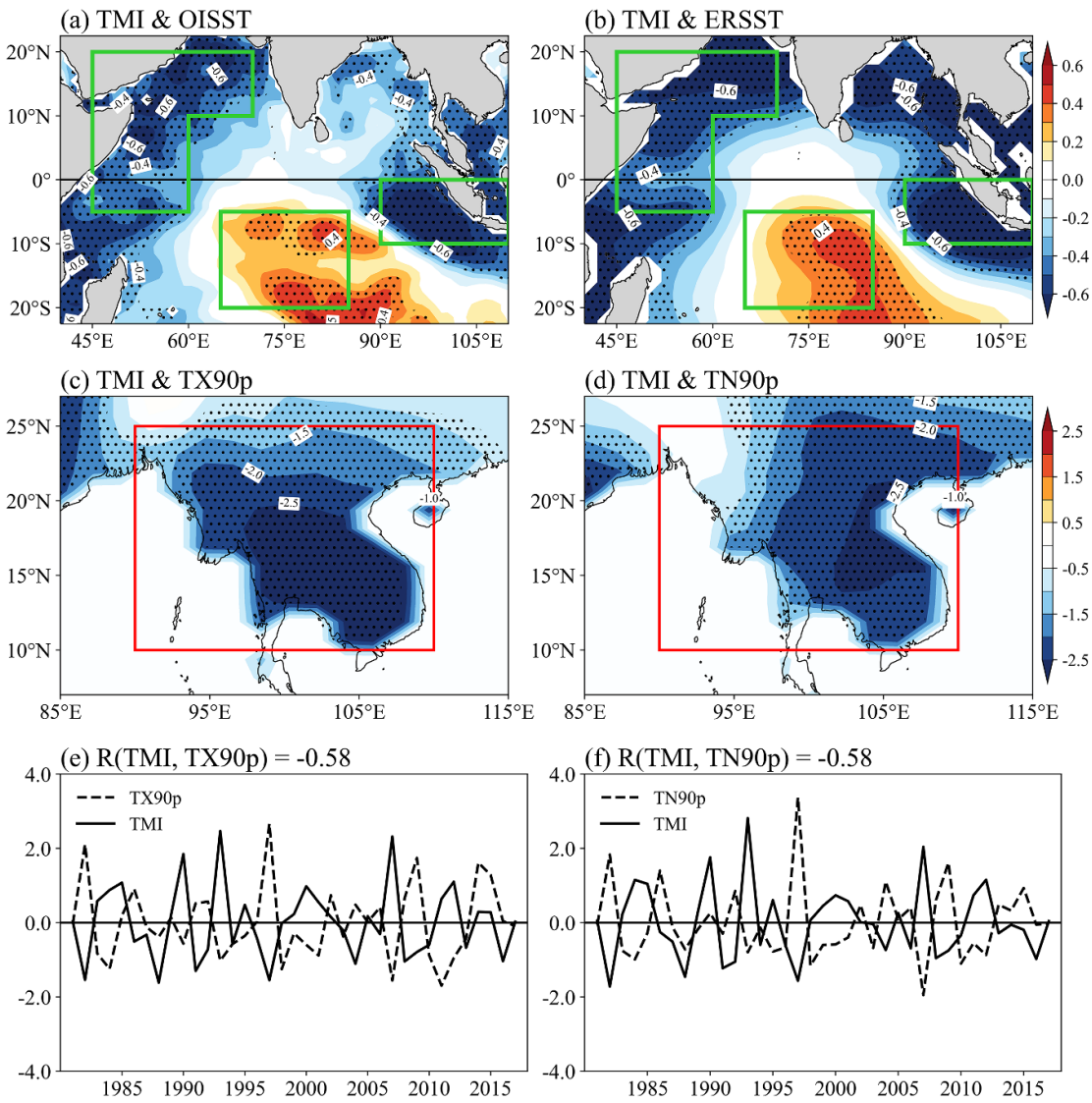

Figure 1. Regressions of (a) the SST anomalies over the tropical Indian Ocean (OISST) and (c) warm days (TX90p) over the Indochina Peninsula on the TMI in JJA for the period of 1982–2018. (b), (d) as (a), (c), but using the SST anomalies from ERSST v5 and warm nights (TN90p). (e) Time series of the TMI (sloid line, green boxes in (a) and from OISST dataset) and area-averaged TX90p (dashed line) over the Indochina Peninsula (red box in (c)). Correlation between the two time-series is −0.58 (significance at 99% confidence level). (f) As (e), but using ERSST v5 for TMI and TN90p (−0.58, significance at 99% confidence level). The black stippled areas in (a)–(d) indicate the significant at 90% confidence level. The green boxes in (a), (b) denote the central tropical (65°–85° E, 5°–20° S), southeastern (90°–110° E, 10° S–0°), and western (45°–60° E, 5° S–20° N and 60°–70° E, 10°–20° N) sectors of the Indian Ocean. The red boxes in (c, d) denote the Indochina Peninsula region (10°–25° N, 90°–110° E).

Figures 4(a) and (b) exhibit the spatial distribution of IOT in relation to precipitation anomalies in the surrounding areas of the tropical Indian Ocean. A remarkable tripole pattern in the precipitation anomalies also occurs over the tropical Indian Ocean in the tropical Indian Ocean (figures 4(a) and (b)), demonstrating the significant influence of the IOT on the precipitation in the tropical Indian Ocean. Meanwhile, there are two obvious cross-equatorial currents along the coasts of the tropical eastern and western Indian Ocean, which enhance the westerly water vapor transport in the northern Indian Ocean and then favor the water vapor convergence in the Indochina Peninsula, further contributing to the development of the local upward movement and leading to the increase of the precipitation anomalies (figures 4(a) and (b)).

To further examine the impact of IOT on circulation anomalies over the Indochina Peninsula, the Rossby wave ray-tracing methods for a horizontally non-uniform basic flow is utilized. Under the prevailing monsoonal winds in JJA, the northward-propagating fluctuations starting from the key regions in the tropical Indian Ocean related to the IOT cross the equator and extent into the northern Indian Ocean (figures 4(c) and (d)),

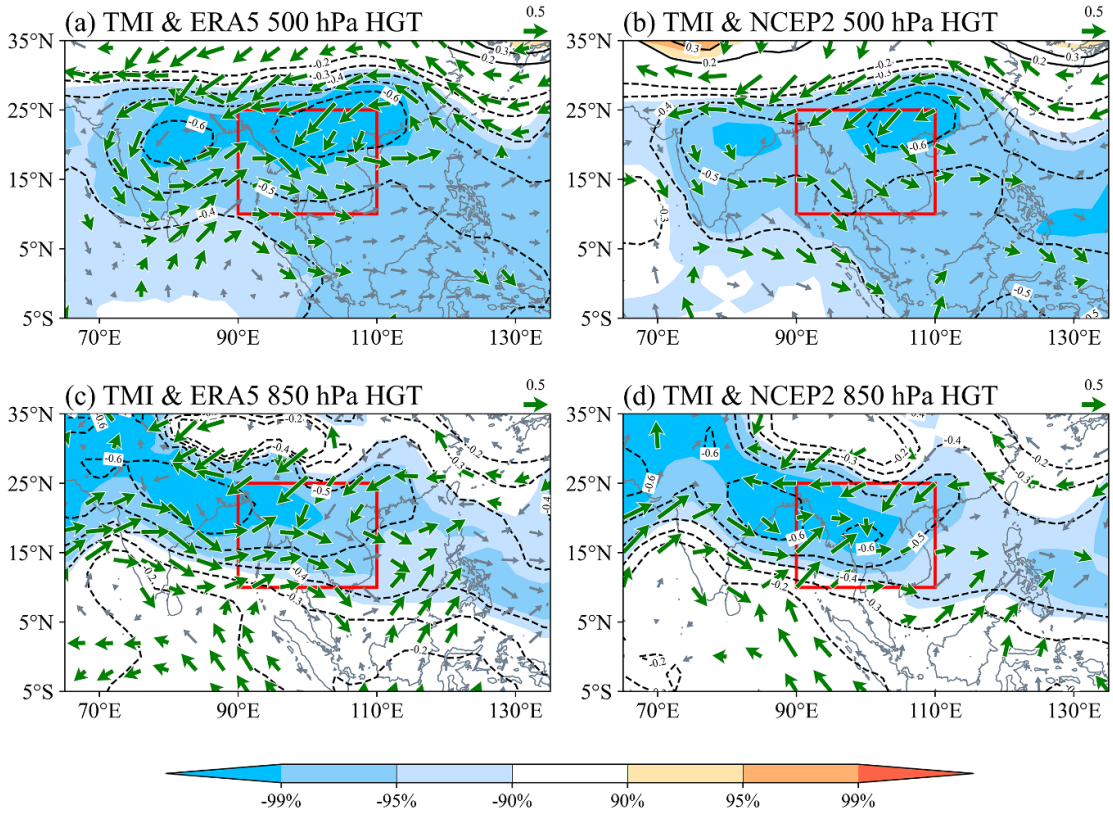

Figure 2. Correlations of the IOT with the geopotential height (HGT, shading) and wind anomalies (vector) at (a) 500 hPa, (c) 850 hPa in JJA using ERA5 dataset. (b), (d) as (a), (c) but using NCEP2 dataset. The colored areas and the green arrow denote the significance above the 90% confidence level. The red boxes denote the Indochina Peninsula region (10°–25° N, 90°–110° E).

thereby influencing the circulation changes over the Indochina Peninsula.

Based on the aforementioned analysis of observational datasets, the IOT modulates the moisture transport via cross-equatorial currents over the Indochina Peninsula, leading to enhanced moisture convergence and increased precipitation. The precipitation-induced anomalous cyclonic circulation further intensifies the local anomalous upward movement. Such circulation configurations promote to decrease of the surface temperatures through stopping solar radiation into the ground, ultimately decreasing the warm extremes days. In summary, the IOT influences local warm extreme events by modulating the anomalous cyclonic circulation over the Indochina Peninsula.

3.3. IOT-induced circulation simulated in numerical experiments

To test the physical mechanism of the IOT on the anomalous circulation in the Indochina Peninsula, the comparative experiments between the control and positive IOT forcing are designed using the CAM5 model (figure 5(a)). The precipitation tripole pattern in the tropical Indian Ocean is responded to the SST anomalies related to the IOT, accompanied with prominent cross-equatorial flows off the coast of the tropical west and east Indian Ocean (figure 5(b)). These two strong cross-equatorial airflows turn into the westerly in the northern Indian Ocean. The carried warm-humid water vapor converges over the Indochina Peninsula and promotes the local upward motion, accompanied with the negative geopotential heigh anomalies occur in the troposphere, thereby leading to the decrease in surface air temperature (figures 5(c) and (d)). These atmosphere circulation responses are well current with the observation, further decreasing the warm extremes in the Indochina Peninsula.

4. Summary and discussion

The Indochina Peninsula experienced the serious extreme temperatures with higher frequency and intensity and relevant droughts in recent decades. The warm extremes (TX90p and TN90p) over the Indochina Peninsula exhibits an obvious interannual variability, which is significantly correlated with the IOT that is an independent ocean-atmosphere coupling mode in the tropical Indian Ocean. Previous studies have reported that the climate variations in many regions, i.e. western United State and Central Siberia, are independently affected by the IOT. In this study, we focused on the interannual variations in the

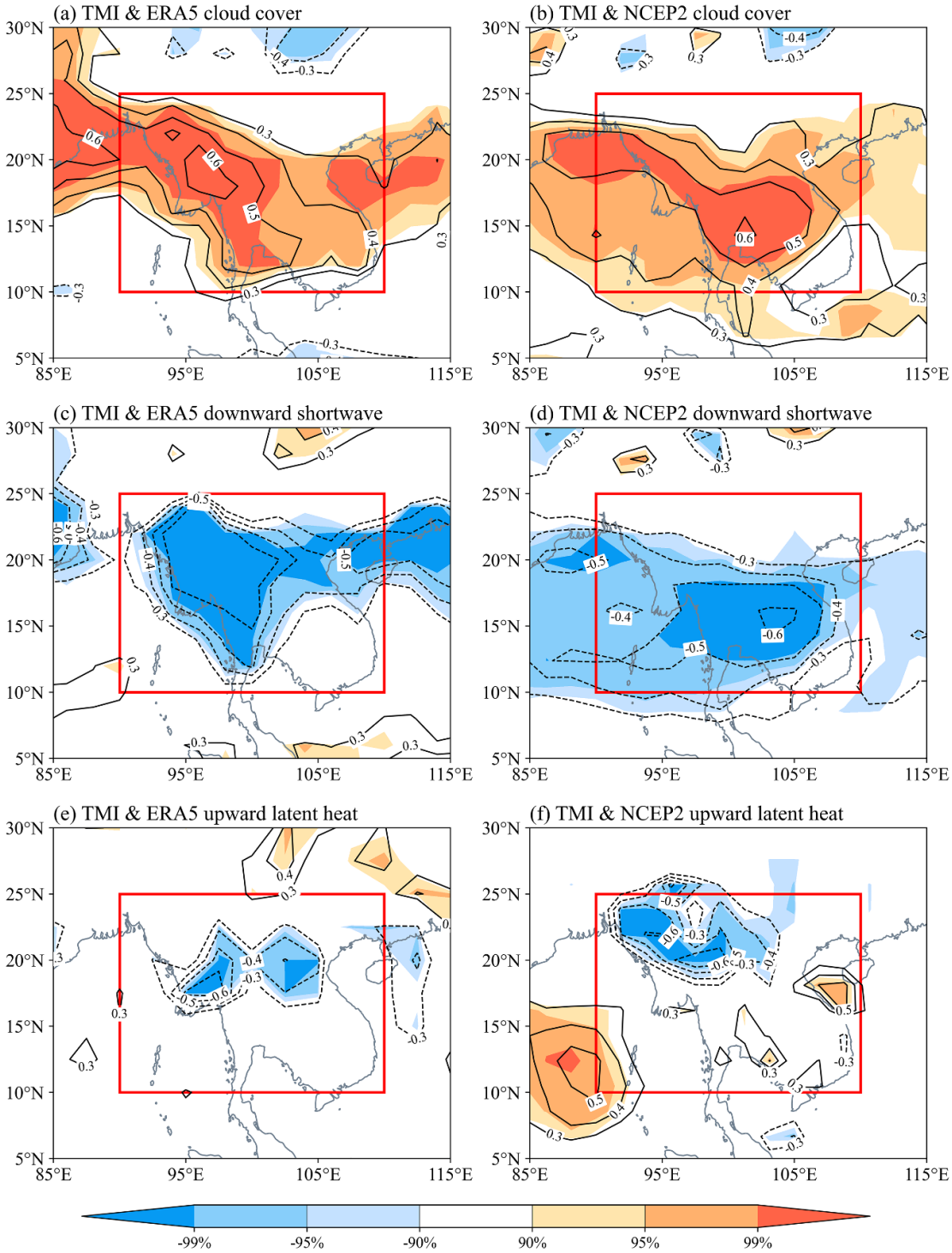

Figure 3. (a) Correlations of the IOT with the total cloud cover in JJA using ERA5 dataset. (c), (e) as (a), but for downward shortwave flux and the upward latent heat flux. (b), (d), (f) as (a), (c), (e), but using NCEP2 dataset. The colored areas denote the significance above the 90% confidence level. The red boxes denote the Indochina Peninsula region (10°–25° N, 90°–110° E).

warm extremes in the Indochina Peninsula linked to the IOT and the underlying physical mechanisms.

The IOT has a temporally and spatially significant negative correlation with summertime temperature extremes in the Indochina Peninsula, which remains significance after removing other climate modes in the Pacific and Indian Oceans. The detailed physical processes through which the IOT influences summer temperature extremes in the Indochina Peninsula are illustrated in figure 6. During positive IOT phase, the

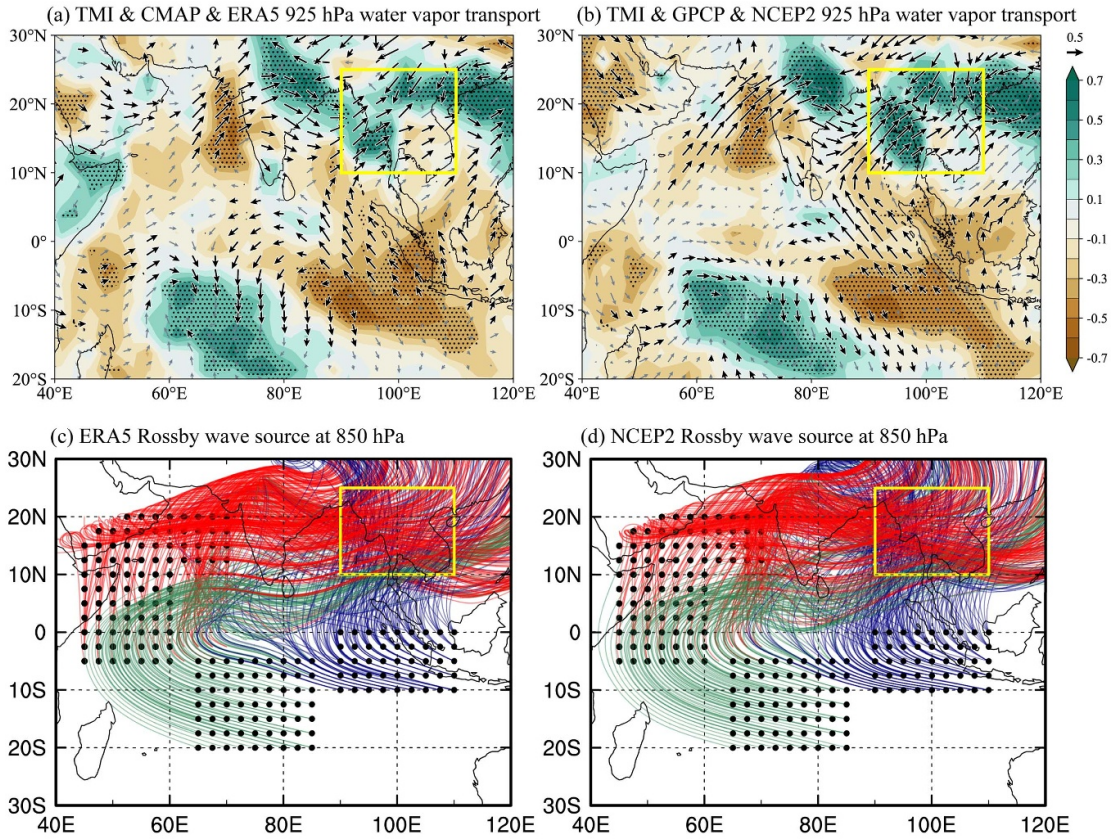

Figure 4. (a) Correlations of the TMI with precipitation (shading) and 950 hPa water vapor transport anomalies (vector) during JJA using ERA5 dataset. The red box denotes the Indochina Peninsula region. The black vectors and the black stippled areas indicate the significant values above the 90% confidence level. (b) as (a), but using NCEP2 dataset. The red boxes denote the Indochina Peninsula region (10°–25° N, 90°–110° E). (c) Stationary Rossby wave trajectories at 850 hPa using ERA5 dataset, (d) as (c) but using NCEP2 dataset. The yellow boxes denote the Indochina Peninsula region (10°–25° N, 90°–110° E).

cross-equatorial airflows tend to strengthen the westerly anomaly in the northern Indian Ocean, favorable for the water vapor convergence and upward motion over the Indochina Peninsula, which correspond the negative geopotential heigh anomalies with an anomalous cyclone. These circulation patterns could affect surface temperature through increasing cloud cover, thus reducing the warm extremes days. These observational atmosphere processes could also be better simulated in CAM5 model.

Our study focuses on the impact of the IOT on extreme temperatures over the Indochina Peninsula. Chu *et al* (2024) reported that both tropical IOB and ENSO could induce anomalous anticyclonic (cyclonic) patterns at the lower (upper) troposphere over the South China Sea, thereby promoting the subsidence and occurrence of interannual variations of extreme high temperatures over the Indochina Peninsula. Additionally, the significant correlations with extreme temperatures over the Indochina Peninsula are also observed in the tropical Atlantic, while the Pacific exhibits signal distinct from ENSO (figure S5). Future studies will comprehensively consider the influences of multiple oceanic regions to refine the mechanistic understanding of extreme temperatures in this region.

Furthermore, the results of the numerical experiments in this study are provided as monthly averaged data, which cannot be directly utilized to calculate extreme temperatures (TX90p/TN90p). Therefore, it is limited to directly verify the impact of IOT on extreme temperatures. Future studies will select CMIP6 models that demonstrate both strong fidelity in simulating the IOT and robust representations of its linkage to regional extremes. Such models may allow for the direct establishment of physical connections between the IOT and extreme high temperatures over the Indochina Peninsula, warranting further in-depth investigation.

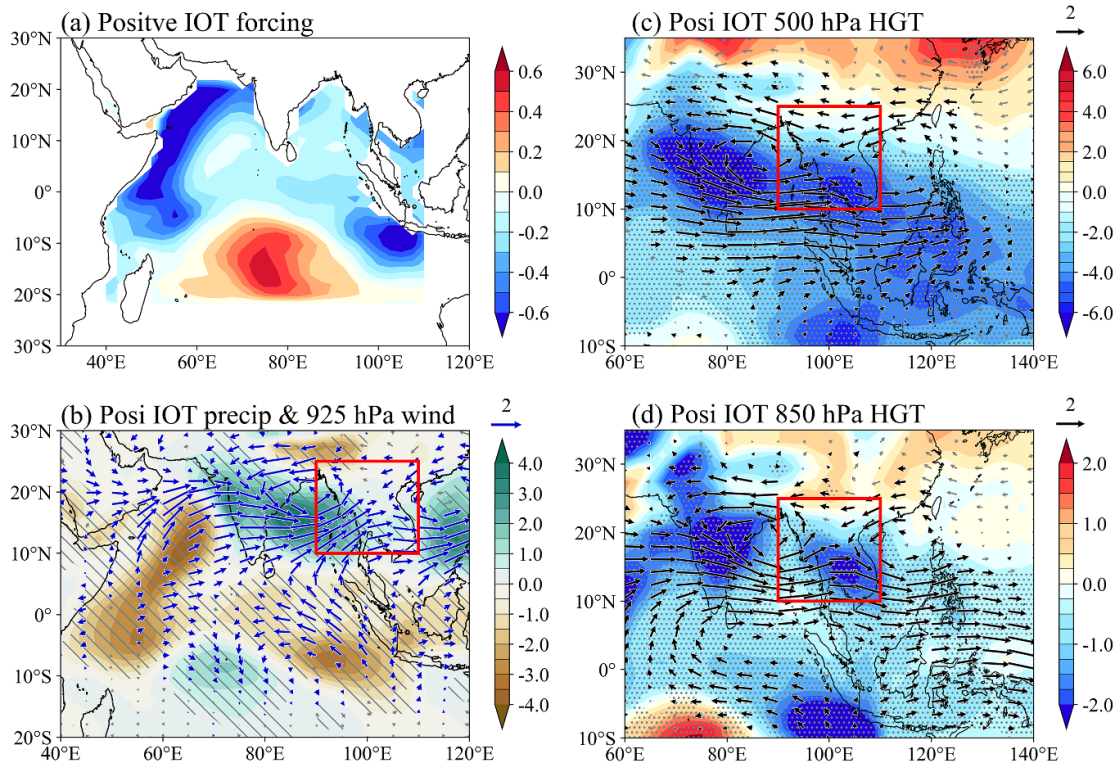

Figure 5. (a) Indian Ocean SST anomalies that were used as the lower boundary conditions for the positive IOT forcing in CAM5 experiments. (b) Differences between the positive IOT forcing simulation and the control simulation for JJA precipitation and 950 hPa wind. The grey slash shade areas and blue vectors in (b) indicate results that are significant above the 95% confidence level. (c), (d) as (b), but for JJA mean geopotential heigh at 500 hPa and surface air temperature. The grey stippled areas and black vectors in (c)–(d) indicate significant values above the 95% confidence level. The red box denotes the Indochina Peninsula region.

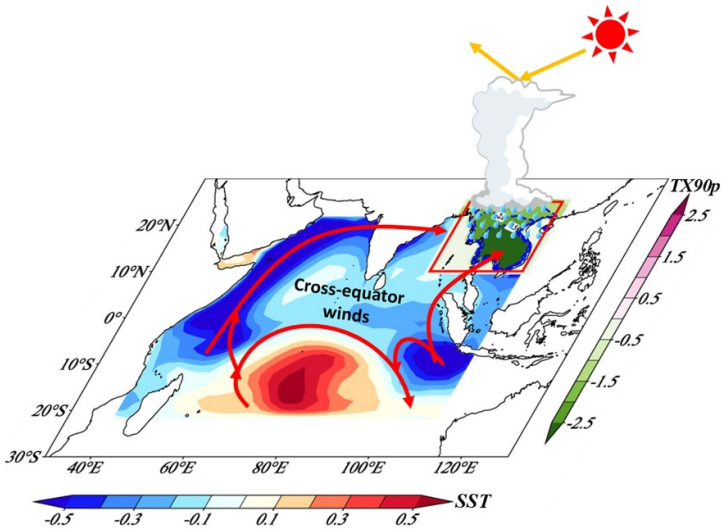

Figure 6. Schematic diagram of the IOT affecting the summer temperature extremes in the Indochina Peninsula during JJA. Red (blue) shadings represent positive (negative) SST anomalies, and green shadings (blue contours) denote the warm extremes (surface temperature). Red arrows (orange vectors) are the anomalous cross-equatorial winds over the tropical Indian Ocean and solar radiation. The cloud with the raindrop indicates the surplus precipitation over the Indochina Peninsula.

Data availability statement

The monthly Optimum Interpolation SST (OISST) and extended Reconstructed SST version 5 (ERSST v5) datasets are both available at https://psl.noaa.gov/data/gridded/tables/sst.html. The monthly mean atmospheric variables were obtained from the National Centers for Environmental Prediction reanalysis 2 (NCEP2; https://psl.noaa.gov/data/gridded/data.ncep.reanalysis2.html) and the European Centre for Medium-Range Weather Forecasts (ECMWF) Reanalysis version

5 (ERA5; www.ecmwf.int/en/forecasts/datasets/reanalysis-datasets/era5). Two monthly indicators for extreme high temperatures TX10p and TN10p are both employed from the World Meteorological Organization (www.metoffice.gov.uk/hadobs/hadex3/download.html). The precipitation datasets were derived from the Climate Prediction Center Merged Analysis of Precipitation (CMAP; https://psl.noaa.gov/data/gridded/data.cmap.html) and the Global Precipitation Climatology Project (GPCP; https://psl.noaa.gov/data/gridded/data.gpcp.html). Community Atmosphere Model (CAM) Version 5 experiment outputs: https://doi.org/10.5281/zenodo.5816581.

All data that support the findings of this study are included within the article (and any supplementary files).

Acknowledgment

Thanks for the Center for Taishan Pandeng Scholar Project, and High Performance Computing and System Simulation, Laoshan Laboratory (Qingdao) for providing computing resource.

Funds

Yazhou Zhang was sponsored by the Shandong Natural Science Foundation Project (ZR2024MD055); Jianping Li was jointly by National Natural Science Foundation of China (NSFC) Project (42130607), Laoshan Laboratory (No. LSKJ202202600); Bin Zuo was supported by the National Natural Science Foundation of China (NSFC) Project (42305187), and South China Sea Institute of Oceanology, Chinese Academy of Sciences (LTO2309).

Conflict of interest

The authors declare no competing interests.

Code availability

The codes used for all the analyses and visualization are available upon reasonable request to the corresponding author.

ORCID iDs

Yazhou Zhang https://orcid.org/0000-0002-6141-8684
Jianping Li https://orcid.org/0000-0003-0625-1575

References

Bretherton C, Widmann M, Dymnikov V, Wallace J and Bladé I 1999 The effective number of spatial degrees of freedom of a time-varying field *J. Clim.* **12** 1990–2009

Chen Z and Li X 2021 Economic impact of transportation infrastructure investment under the belt and road initiative *Asia Eur. J.* **19** 131–59

Cheong W, Timbal B, Golding N, Sirabaha S, Kwan K F, Cinco T A, Archevarahuprok B, Vo V H, Gunawan D and Han S 2018 Observed and modelled temperature and precipitation extremes over South east Asia from 1972 to 2010 *Int. J. Climatol.* **38** 3013–27

Chu C, Fan Y, Yu P, Liu Y, Chen S and Zhou B 2024 Variations of summer extreme high temperatures over the Indochina Peninsula: roles of oceanic systems *Atmos. Res.* **311** 107684

Dang T, Honda Y, Van Do D, Pham A, Chu C, Huang C and Phung D 2019 Effects of extreme temperatures on mortality and hospitalization in Ho Chi Minh City, Vietnam *Int. J. Environ. Res. Public Health* **16** 432

Dong Z, Wang L, Sun Y, Hu T, Limsakul A, Singhruck P and Pimonsree S 2021 Heatwaves in Southeast Asia and their changes in a warmer world *Earth's Future* **9** e2021EF001992

Dunn R *et al* 2020 Development of an updated global land *in situ*-based data set of temperature and precipitation extremes: HadEX3 *J. Geophys. Res. Atmos.* **125** e2019JD032263

Endo S and Tozuka T 2016 Two flavors of the Indian Ocean dipole *Clim. Dyn.* **46** 3371–85

Fan L and Meng X 2023 The asymmetric predictive power of Indian Ocean dipole for subsequent year's ENSO: role of Atlantic Ocean as an intermediary *Geophys. Res. Lett.* **50** e2023GL105525

Fan Y, Li J, Zhu S, Li H and Zhou B 2022 Trends and variabilities of precipitation and temperature extremes over Southeast Asia during 1981–2017 *Meteorol. Atmos. Phys.* **134** 78

Hersbach H *et al* 2020 The ERA5 global reanalysis *Q. J. R. Meteorol. Soc.* **146** 1999–2049

Hoskins B and Karoly D 1981 The steady linear response of a spherical atmosphere to thermal and orographic forcing *J. Atmos. Sci.* **38** 1179–96

Hrudya P, Varikoden H and Vishnu R 2021 review on the Indian summer monsoon rainfall, variability and its association with ENSO and IOD *Meteorol. Atmos. Phys.* **133** 1–14

Huang B, Thorne P, Banzon V, Boyer T, Chepurin G, Lawrimore J, Menne M, Smith T, Vose R and Zhang H 2017 Extended reconstructed sea surface temperature, version 5 (ERSSTv5): upgrades, validations, and intercomparisons *J. Clim.* **30** 8179–205

Huang C, Cheng J, Phung D, Tawatsupa B, Hu W and Xu Z 2018 Mortality burden attributable to heatwaves in Thailand: a systematic assessment incorporating evidence-based lag structure *Environ. Int.* **121** 41–50

Huffman G, Bolvin D, Nelkin E and Adler R 2015 *GPCP Version 2.2 Combined Precipitation Data Set* (Research Data Archive at the National Center for Atmospheric Research, Computational and Information Systems Laboratory)

Kanamitsu M, Ebisuzaki W, Woollen J, Yang S, Hnilo J, Fiorino M and Potter G 2002 NCEP–DOE AMIP-II reanalysis (R-2) *Bull. Am. Meteorol. Soc.* **83** 1631–44

Karoly D 1983 Rossby wave propagation in a barotropic atmosphere *Dyn. Atmos. Oceans* **7** 111–25

Li J, Li F, He S, Wang H and Orsolini Y 2021 The Atlantic multidecadal variability phase dependence of teleconnection between the North Atlantic oscillation in february and the Tibetan Plateau in march *J. Clim.* **34** 4227–42

Li J, Sun C and Jin F 2013 NAO implicated as a predictor of Northern Hemisphere mean temperature multidecadal variability *Geophys. Res. Lett.* **40** 5497–502

Li J, Zheng F, Sun C, Feng J and Wang J 2019 Pathways of influence of the Northern Hemisphere mid–high latitudes on East Asian climate: a review *Adv. Atmos. Sci.* **36** 902–21

Li L and Nathan T 1997 Effects of low-frequency tropical forcing on intraseasonal tropical–extratropical interactions *J. Atmos. Sci.* **54** 332–46

Li X 2020 Heat wave trends in Southeast Asia during 1979–2018: the impact of humidity *Sci. Total Environ.* **721** 137664

Li Y and Li J 2012 Propagation of planetary waves in the horizonal non-uniform basic flow (in Chinese) *Chin. J. Geophys.* **55** 361–71
Li Y, Li J, Jin F and Zhao S 2015 Interhemispheric propagation of stationary rossby waves in a horizontally nonuniform background flow *J. Atmos. Sci.* **72** 3233–56
Lin L, Chen C and Luo M 2018 Impacts of El Niño-Southern Oscillation on heat waves in the Indochina peninsula *Atmos. Sci. Lett.* **19** e856
Liu H, Tan K and Lim G 2021 Introduction—Southeast Asia and the belt and road initiative: the political economy of regionalism, trade, and infrastructure *Singap. Econ. Rev.* **66** 1–20
Luo M and Lau N 2018 Synoptic characteristics, atmospheric controls, and long-term changes of heat waves over the Indochina Peninsula *Clim. Dyn.* **51** 2707–23
Matthews T, Wilby R and Murphy C 2017 Communicating the deadly consequences of global warming for human heat stress *Proc. Natl Acad. Sci. USA* **114** 3861–6
Mora C *et al* 2017 Global risk of deadly heat *Nat. Clim. Change* **7** 501–6
North G, Bell T, Cahalan R and Moeng F 1982 Sampling errors in the estimation of empirical orthogonal functions *Mon. Weather Rev.* **110** 699–706
Räsänen T, Lindgren V, Guillaume J, Buckley B and Kummu M 2016 On the spatial and temporal variability of ENSO precipitation and drought teleconnection in mainland Southeast Asia *Clim. Past* **12** 1889–905
Reynolds R, Rayner N, Smith T, Stokes D and Wang W 2002 An improved *in situ* and satellite SST analysis for climaate *J. Clim.* **15** 1609–25
Sun C, Li J and Ding R 2016 Strengthening relationship between ENSO and Western Russian summer surface temperature *Geophys. Res. Lett.* **43** 843–51
Tang K 2019 Climate change in Malaysia: trends, contributors, impacts, mitigation and adaptations *Sci. Total Environ.* **650** 1858–71
Tebaldi C and Lobell D 2018 Estimated impacts of emission reductions on wheat and maize crops *Clim. Change* **146** 533–45
Thirumalai K, DiNezio P, Okumura Y and Deser C 2017 Extreme temperatures in Southeast Asia caused by El Niño and worsened by global warming *Nat. Commun.* **8** 15531
Tritto A and Camba A 2022 The belt and road initiative in Southeast Asia: a mixed methods examination *J. Contemp. China* **32** 436–54
Wang H, Li J, Zheng F and Li F 2023 The synergistic effect of the summer NAO and northwest pacific SST on extreme heat events in the central–eastern China *Clim. Dyn.* **61** 4283–300
Wang H, Zheng F, Diao Y, Li J, Sun R, Tang X, Sun Y, Li F and Zhang Y 2022 The synergistic effect of the preceding winter Northern Hemisphere annular mode and spring tropical North Atlantic SST on spring extreme cold events in the mid-high latitudes of East Asia *Clim. Dyn.* **59** 3175–91
Whitham G 1960 A note on group velocity *J. Fluid Mech.* **9** 347–52
Xie P and Arkin P 1997 Global precipitation: a 17-year monthly analysis based on gauge observations, satellite estimates, and numerical model outputs *Bull. Am. Meteorol. Soc.* **78** 2539–58
Xie S, Hu K, Hafner J, Tokinaga H, Du Y, Huang G and Sampe T 2009 Indian Ocean capacitor effect on Indo–Western Pacific climate during the Summer following El Niño *J. Clim.* **22** 730–47
Yang J, Liu Q, Xie S, Liu Z and Wu L 2007 Impact of the Indian Ocean SST basin mode on the Asian summer monsoon *Geophys. Res. Lett.* **34** L02708
Yu S, Fan L, Zheng X, Zhang Y, Zhou Z and Li Z 2023 Sources of inter-model diversity in the strength of the relationship between the Indian Summer Monsoon Rainfall and El Niño-Southern oscillation *Geophys. Res. Lett.* **50** e2022GL101718
Zampieri M, Ceglar A, Dentener F and Toreti A 2017 Wheat yield loss attributable to heat waves, drought and water excess at the global, national and subnational scales *Environ. Res. Lett.* **12** 064008
Zander K, Richerzhagen C and Garnett S 2019 Human mobility intentions in response to heat in urban South East Asia *Glob. Environ. Change* **56** 18–28
Zhang L, Chen Z and Zhou T 2021a Human influence on the increasing drought risk over Southeast Asian monsoon region *Geophys. Res. Lett.* **48** e2021GL093777
Zhang Y, Li J, Diao Y, Hou Z and Liu T 2022b Influence of the tropical Indian Ocean tripole on summertime cold extremes over Central Siberia *Geophys. Res. Lett.* **49** e2022GL100709
Zhang Y, Li J, Hou Z, Zuo B, Xu Y, Tang X and Wang H 2022a Climatic effects of the Indian Ocean tripole on the Western United States in boreal summer *J. Clim.* **35** 2503–23
Zhang Y, Li J, Xue J, Feng J, Wang Q, Xu Y, Wang Y and Zheng F 2018 Impact of the south China sea summer monsoon on the Indian Ocean dipole *J. Clim.* **31** 6557–72
Zhang Y, Li J, Zhao S, Zheng F, Feng J, Li Y and Xu Y 2020 Indian Ocean tripole mode and its associated atmospheric and oceanic processes *Clim. Dyn.* **55** 1367–83
Zhang Y, Li J, Zheng F, Yu M, Feng J and Sun C 2021 Impact of the South China Sea Summer Monsoon on the Indian Ocean dipole in CMIP5 models *J. Clim.* **34** 1963–81
Zhao S, Li J and Li Y 2015 Dynamics of an interhemispheric teleconnection across the critical latitude through a southerly duct during boreal winter *J. Clim.* **28** 7437–56
Zhao S, Li J, Li Y, Jin F and Zheng J 2019 Interhemispheric influence of Indo-Pacific convection oscillation on Southern Hemisphere rainfall through southward propagation of Rossby waves *Clim. Dyn.* **52** 3203–21
Zhu M, Zhang Y, Li J, Liu T, Hou Z and Wang H 2024 Physical connection between the tropical Indian Ocean tripole and western Tibetan Plateau surface air temperature during boreal summer *Clim. Dyn.* **62** 9703–18